J Arid Land (2023) 15(6): 649–666
https://doi.org/10.1007/s40333-023-0057-9

Science Press Springer-Verlag

Aeolian activity in the southern Gurbantunggut Desert of China during the last 900 years

LI Wen[1,2], MU Guijin[3*], YE Changsheng[2], XU Lishuai[4], LI Gen[2]

[1] Key Laboratory for Digital Land and Resources of Jiangxi Province, East China University of Technology, Nanchang 330013, China;
[2] School of Earth Sciences, East China University of Technology, Nanchang 330013, China;
[3] Xinjiang Institute of Ecology and Geography, Chinese Academy of Sciences, Urumqi 830011, China;
[4] College of Resources and Environment, Shanxi Agricultural University, Jinzhong 030801, China

Abstract: The mineral dust emitted from Central Asia has a significant influence on the global climate system. However, the history and mechanisms of aeolian activity in Central Asia remain unclear, due to the lack of well-dated records of aeolian activity and the intense wind erosion in some of the dust source areas (e.g., deserts). Here, we present the records of aeolian activity from a sedimentary sequence in the southern Gurbantunggut Desert of China using grain size analysis and optically stimulated luminescence (OSL) dating, based on field sampling in 2019. Specifically, we used eight OSL dates to construct chronological frameworks and applied the end-member (EM) analysis for the grain size data to extract the information of aeolian activity in the southern Gurbantunggut Desert during the last 900 a. The results show that the grain size dataset can be subdivided into three EMs (EM1, EM2, and EM3). The primary modal sizes of these EMs (EM1, EM2, and EM3) are 126.00, 178.00, and 283.00 μm, respectively. EM1 represents a mixture of the suspension components and saltation dust, while EM2 and EM3 show saltation dust transported over a shorter distance via strengthened near-surface winds, which can be used to trace aeolian activity. Combined with the OSL chronology, our results demonstrate that during the last 900 a, more intensive and frequent aeolian activity occurred during 450–100 a BP (Before Present) (i.e., the Little Ice Age (LIA)), which was reflected by a higher proportion of the coarse-grained components (EM2+EM3). Aeolian activity decreased during 900–450 a BP (i.e., the Medieval Warm Period (MWP)) and 100 a BP–present (i.e., the Current Warm Period (CWP)). Intensified aeolian activity was associated with the strengthening of the Siberian High and cooling events at high northern latitudes. We propose that the Siberian High, under the influence of temperature changes at high northern latitudes, controlled the frequency and intensity of aeolian activity in Central Asia. Cooling at high northern latitudes would have significantly enhanced the Siberian High, causing its position to shift southward. Subsequently, the incursion of cold air masses from high northern latitudes resulted in stronger wind regimes and increased dust emissions from the southern Gurbantunggut Desert. It is possible that aeolian activity may be weakened in Central Asia under future global warming scenarios, but the impact of human activities on this region must also be considered.

Keywords: aeolian activity; grain size; wind regime; Little Ice Age; Siberian High; climatic drying; Central Asia

Citation: LI Wen, MU Guijin, YE Changsheng, XU Lishuai, LI Gen. 2023. Aeolian activity in the southern Gurbantunggut Desert of China during the last 900 years. Journal of Arid Land, 15(6): 649–666. https://doi.org/10.1007/s40333-023-0057-9

*Corresponding author: MU Guijin (E-mail: gjmu@ms.xjb.ac.cn)
Received 2022-09-14; revised 2022-12-25; accepted 2023-01-03

1 Introduction

In arid and semi-arid regions, frequent and intensive aeolian activity, such as dust storms, may lead to meteorological disasters with major adverse impacts on human livelihood and health (Middleton and Sternberg, 2013). Additionally, the aeolian activity in arid regions can result in the emission of large quantities of mineral dust that exerts a significant influence on the global climate via balancing atmospheric radiation (Tegen et al., 1996; Huang et al., 2006), and regulating atmospheric CO_2 (Martin and Fitzwater, 1988; McTainsh and Strong, 2007) and radiation balance on the Earth's surface (Ginoux et al., 2004; Maher et al., 2010; Booth et al., 2012). Central Asia is located far from oceanic moisture sources; it contains one of the largest hyper-arid regions on Earth and is one of the largest global dust source areas (Li et al., 2022). Ginoux et al. (2004) estimated that approximately 25.00% of global dust emissions are sourced from the interior of Asia. The dust materials can be transported and dispersed by wind and deposited downwind across large regions, such as East Asia (Fang and Li, 1999; Lu et al., 2021), and the North Pacific and Greenland (Porter, 2001; Zhang, 2001), with influences on the global climate and biogeochemical cycles. The strong correlation of the increased dust accumulation in the desert regions of western China and grain size coarsening in the loess sequences in East Asia (e.g., the Chinese Loess Plateau) with the increased content of microparticles in Greenland ice cores shows that the dust emitted from the interior of Asia has a global-scale influence on both climate change and the circulation of materials (Rea, 1994; Zielinski and Mershon, 1997; Fang and Li, 1999; Zhang, 2001; Ginoux et al., 2004; Zhang et al., 2018; Lu et al., 2021; Shin et al., 2021). A comprehensive understanding of the processes responsible for the formation, mobilization, and transportation of dust is the foundation of attempts to prevent and mitigate the adverse consequences of aeolian activity. Thus, dust emission and transportation have attracted significant research interest during the last few decades (Qiang et al., 2007; Chen et al., 2013; He et al., 2015; Li et al., 2019).

Changes in aeolian activity on different time scales in Central Asia have been reconstructed from various geological archives and instrumental records (Huang et al., 2011; Chen et al., 2013; Xu, 2014; Han et al., 2019; Zhou et al., 2019; Qiang et al., 2022). These results show that the most frequent and intense aeolian activity occurred during cold climatic intervals. For instance, on the southern margin of the Tarim Basin, Xinjiang Uygur Autonomous Region, China (Han et al., 2019) and in the northeastern Qinghai-Tibet Plateau, China (Qiang et al., 2014), the intervals of intensified dust storms during the Holocene coincided with increased ice rafting (i.e., cold events) in the North Atlantic. However, a case study from Jili Lake in North Xinjiang indicated that during the last 1600 a, intensified or weakened aeolian activity occurred in the Medieval Warm Period (MWP) or Little Ice Age (LIA) (Qiang et al., 2022). Regarding the processes of dust formation, emission, and transportation, it has been assumed that climatic drying expands the dust source areas, leading to the strengthening of aeolian activity (Rea and Leinen, 1988; Guo et al., 2002). It has also been argued that wind strength plays an essential role in the emission, transportation, and deposition of dust (Kurosaki and Mikami, 2003; Liu et al., 2004; Qiang et al., 2007). Additionally, changes in the frequency and intensity of aeolian activity are controlled by the surface wind velocity, which is influenced by the atmospheric circulation system (Chen et al., 2013; Xu et al., 2018). However, the relationship of aeolian activity with climatic conditions and atmospheric circulation systems is not always fixed. For example, in the Gonghe Basin on the northeastern Qinghai-Tibet Plateau, a trend of weakening aeolian activity occurred in the early to middle Holocene due to increased regional moisture and vegetation cover. In contrast, during the late Holocene, abrupt and intense episodes of aeolian activity were driven by increased wind velocity (Qiang et al., 2014).

Most geological studies on past dust activity have focused on the major downwind dust archives, such as lake, peat, and loess sediments (An et al., 2011; Huang et al., 2011; Chen et al., 2013; Xu, 2014; Han et al., 2019; Li et al., 2019; Zhou et al., 2019; Qiang et al., 2022; Su et al., 2023). However, geological records of aeolian activity are scarce in the dust source areas

themselves. Desert deposits, which are most frequently, directly, and strongly affected by aeolian activity, have been neglected because of the lack of well-dated records and substantial wind erosion. As mentioned above, understanding the history and driving mechanisms of aeolian activity in Central Asia is of major scientific and practical significance. However, several major issues remain unresolved, including the response of aeolian activity to climate warming (e.g., during the MWP) or cooling (e.g., during the LIA); these issues have important implications for predicting the course of aeolian activity under current and future global climate warming. Additionally, determining the main factors controlling aeolian activity is also essential for the monitoring, prevention, and mitigation of major dust storms. To address these issues, we studied three aeolian sections in the southern Gurbantunggut Desert in Xinjiang of China, which is one of the major dust source areas in Central Asia (Li et al., 2022). Specifically, we used grain size analysis combined with optically stimulated luminescence (OSL) dating to reconstruct the history of aeolian activity over the past 900 a and determine its driving mechanisms. The purpose of this study is to characterize the evolution history and driving mechanisms of aeolian activity in Central Asia. The information of formation, mobilization, and transportation of aeolian activity obtained by this study would also provide insights into the prevention and mitigation of the adverse consequences of dust emissions in Central Asia.

2 Materials and methods

2.1 Study area

The Gurbantunggut Desert (44°11′–46°20′N, 84°31′–90°00′E), which is the second largest desert in China and has the area of 4.88×10^4 km^2, is located within the central Junggar Basin, Xinjiang, China (Fig. 1). It is bounded by the Tianshan Mountains to the south and the Altay Mountains to the northeast (Wang et al., 2005; Li and Fan, 2011; Li et al., 2022). The Junggar Basin is characterized by an arid continental climate. According to the observed data from Mosuowan meteorological station, the mean annual precipitation in the Gurbantunggut Desert is 123.61 mm, the mean annual potential evaporation is 1940.59 mm, and the annual mean temperature is 6.65°C

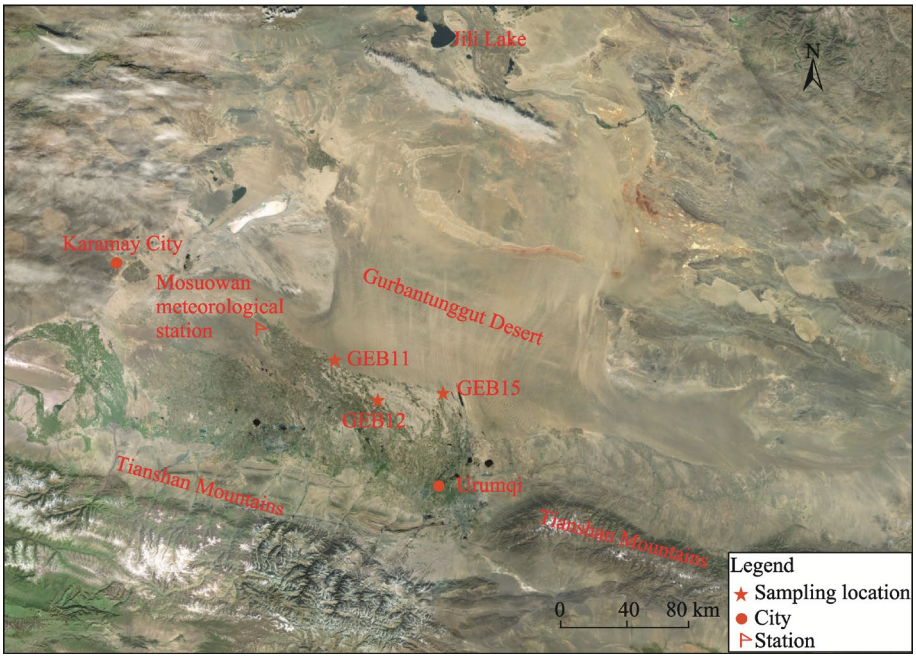

Fig. 1 Satellite image showing the sampling locations of profiles GEB11 (44°48′N, 86°37′E), GEB12 (44°41′N, 86°45′E), and GEB15 (44°42′N, 87°21′E) in the southern Gurbantunggut Desert. The image was downloaded from the National Platform for Common Geospatial Information Services (https://www.tianditu.gov.cn/).

(Qian and Wu, 2010). During the last few decades, temperature and precipitation in the Gurbantunggut Desert have shown an increasing trend (Liu, 2020) (Fig. 2). The wind regimes of the Gurbantunggut Desert are mainly governed by the Siberian High and the Westerlies. Specifically, in winter, the climate is controlled by the western branch of the Siberian High, with northeast winds prevailing in the northeastern and central parts of the desert, and northwest winds prevailing in the western and southern parts; in summer, the desert is influenced by the northern branch of the Westerlies (Wang et al., 2005; Li et al., 2022).

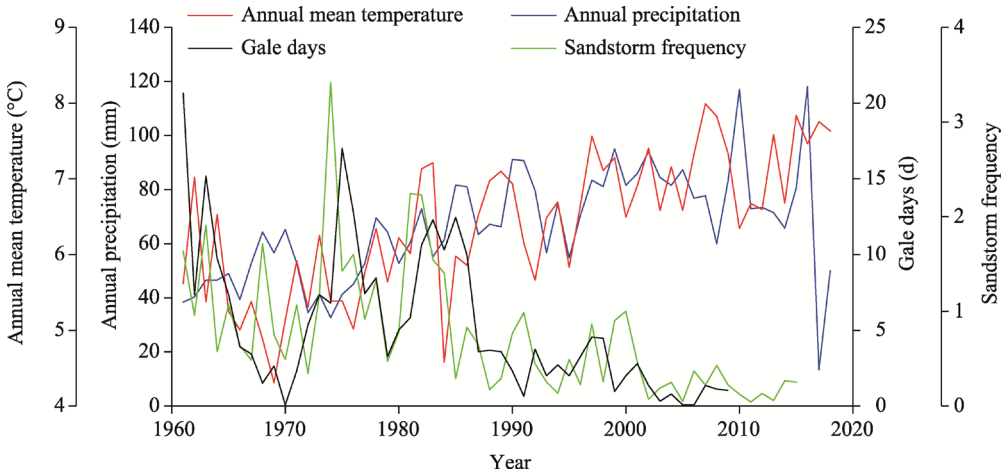

Fig. 2 Variations in temperature and precipitation from 1961 to 2018 in the Gurbantunggut Desert (data from Liu (2020)), the number of gale days from 1961 to 2009 in the southern Gurbantunggut Desert (data from Yu et al. (2011)), and sandstorm frequency from 1961 to 2015 in the North Xinjiang (data from Li and Tang (2017)).

2.2 Samples and methods

2.2.1 Field sampling

Field surveys of the aeolian deposits were carried out in the southern Gurbantunggut Desert in 2019. It should be noted that the Gurbantunggut Desert has the highest vegetation coverage of any desert on Earth. During field work we found that the dominant plant species on the top of the dunes and in the interdune areas is *Haloxylon ammonium* (Fig. 3). Aeolian activity is the

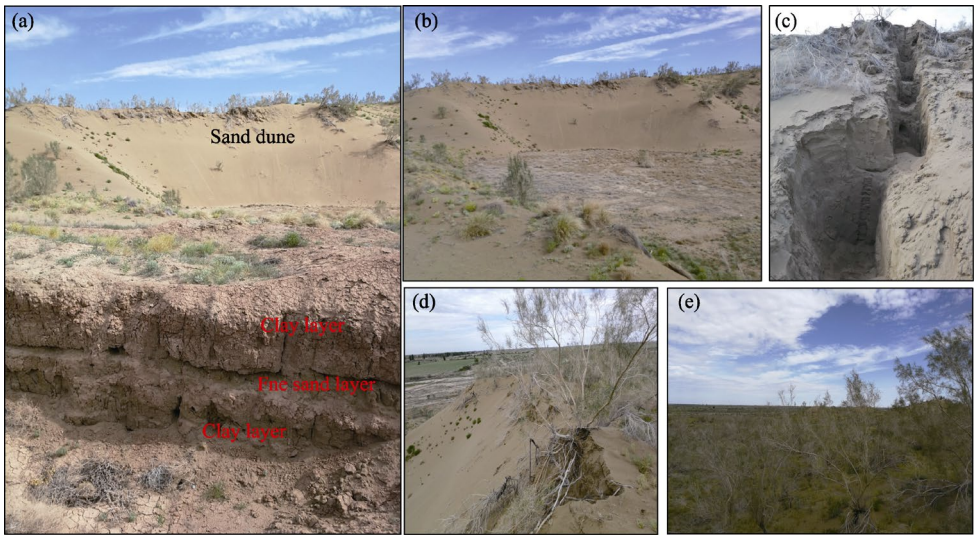

Fig. 3 Photographs showing the field area. (a and b), sand dunes and the underlying clay strata; (c), profile GEB11; (d and e), the dominant plant species (*Haloxylon ammodendron*) growing on the top of the dunes and in the interdune areas, respectively.

dominant geomorphological process in the study area, since we observed no evidence of any other processes, such as fluvial erosion. Three sand dunes (GEB11 (44°48′N, 86°37′E), GEB12 (44°41′N, 86°45′E), and GEB15 (44°42′N, 87°21′E); Fig. 1) were selected for stratigraphic profile analysis. Profile GEB11 is the main research object of the present study, while profiles GEB12 and GEB15 provide supplementary information. Our field surveys confirmed that profile GEB11 accumulated continuously from the base to the surface, and there was no evidence of abrupt changes. In contrast, profiles GEB12 and GEB15 showed evidence of sedimentary hiatuses and/or abrupt stratigraphic changes. Details of the three profiles are described in Table 1.

Table 1 Detailed information of profiles GEB11, GEB12, and GEB15 selected in this study

Profile	Depth (cm)	Detailed information of stratum	Detailed information of sediment and OSL dating samples
GEB11	0–80	Gray fine sand with abundant plant roots. The top 15 cm layer contained horizontal bedding, while the 15–80 cm layer lacked well-defined bedding.	Totally 70 sediment samples were sampled at 10-cm intervals, and 4 OSL dating samples were sampled at the depths of 100, 300, 500, and 700 cm, respectively.
	80–200	Gray fine sand with occasional roots and well-developed oblique bedding.	
	200–600	Ale-gray fine sand with no clear bedding. Occasional roots were observed at the depths of 320–330, 410–440, and 480–500 cm.	
	600–700	Gray fine sand with horizontal bedding and low soil water content.	
GEB12	0–105	Gray fine sand with abundant plant roots and well-developed horizontal bedding. The interval of 90–105 cm depth contained occasional traces of white calcareous cement.	Totally 34 sediment samples were sampled at 5-cm intervals, and 2 OSL dating samples were sampled at the depths of 100 and 140 cm, respectively.
	105–120	Dark-red clay with well-developed horizontal bedding; 120–140 cm depth: greyish-green fine sand with a flat upper surface and well-developed horizontal bedding.	
	140–170	Clay fine silt with black rusty mottles. The intervals of 140–155 and 155–170 cm depths were dark red and grayish-yellow, respectively.	
GEB15	0–140	Gray fine sand with well-developed bedding and occasional plant roots.	Totally 39 sediment samples were sampled at 5-cm intervals, and 2 OSL dating samples were sampled at the depths of 130 and 160 cm, respectively.
	140–195	Dark red clay with a flat upper surface and thin horizontal bedding.	

Note: GEB11 (44°48′N, 86°37′E), GEB12 (44°41′N, 86°45′E), and GEB15 (44°42′N, 87°21′E) are selected sand dunes. OSL, optically stimulated luminescence.

2.2.2 Laboratory methods

The grain sizes of 70 samples from profile GEB11 were determined in Xinjiang Institute of Ecology and Geography, Chinese Academy of Sciences in Urumqi, China. These samples were prepared by removing organic matter and carbonates with 10 mL of 30% H_2O_2 and 10 mL of 10% HCl, respectively. After rinsing with distilled water, 10 mL of 0.05 mol/L $(NaPO_4)_6$ was added to aid dispersion, and grain sizes were determined using Mastersizer 2000 Laser Diffraction Particle-size Analyzer (Malvern Instruments Ltd., Worcestershire, UK) with the measurement range of 0.02–2000.00 μm. Grain size distributions were classified as clay (<4.00 μm (>8φ, where φ= $-\log_2(D)$, in which D is the diameter, with the unit of mm)), silt (4.00–63.00 μm (8φ–4φ)), very fine sand (63.00–125.00 μm (4φ–3φ)), fine sand (125.00–250.00 μm (3φ–2φ)), medium sand (250.00–500.00 μm (2φ–1φ)), and coarse sand (500.00–1000.00 μm (1φ–0φ)).

We determined the chronologies of the three profiles based on optically stimulated luminescence (OSL) dating. Eight OSL samples collected from the three profiles (GEB11-1, GEB11-3, GEB11-5, GEB11-7, GEB12-2, GEB12-3, GEB15-2, and GEB15-3) were measured at the Institute of Geology, China Earthquake Administration in Beijing, China. Samples were prepared under subdued red light (661 nm) in the laboratory. The outermost 2–3 cm sediment layer of these samples was removed, and the materials in the central part of the sample tubes that had not been exposed to light, was treated with H_2O_2 to remove organic matter and then with HCl

to remove carbonates. Pure quartz grains within the size range of 90.00–180.00 μm were extracted for equivalent dose determination. Hydrofluoric acid (HF) was used to separate quartz and feldspar. De measurements were carried out using a Risø TL/OSL Reader Model DA-20 R4 automatic measurement system (Risø, Copenhagen, Denmark) equipped with blue diodes (k=470 (±5) nm, where k is the wave length) and a $^{90}Sr/^{90}Y$ radioactive beta source. The luminescence was also detected using a U-340 filter (Risø, Copenhagen, Denmark). The materials from the ends of the tube was used to measure the concentrations of U, Ra, Th, and K using a GEM70 P4-95 P-type Ge-ray spectrometer (Ortec, Oak Ridge, USA). The soil water contents were measured by weighing the samples before and after drying in Institute of Geology, China Earthquake Administration in Beijing, China.

2.2.3 Data analysis

Generally, grain size composition of sediments is affected by multiple transport processes or provenances. In this study, we used the end-member (EM) analysis of the grain size data implemented with AnalySize software (Paterson and Heslop, 2015) in a MATLAB GUI (Mathworks, Natick, USA) to extract the effective information about aeolian activity. We further determined the minimum number of EMs based on the coefficient of determination (R^2), angular deviation, and reconstruction (degree) (Paterson and Heslop, 2015) to provide goodness-of-fit statistics. The higher values of R^2 (preferably higher than 0.8) and lower values of angular deviation (preferably lower than 5) indicate a superior degree of fitting, with the EMs providing a better representation of data (Paterson and Heslop, 2015).

3 Results

3.1 OSL dating results

The OSL dating results are presented in Table 2. The bottom of profile GEB11 (about 700 cm depth) has an age of 900 a, and the age is generally in chronological order. The linear age-depth relationship has the correlation coefficient of 0.933 (Fig. 4). The mean sedimentation rate of this profile is 0.778 cm/a, and the sedimentation rate in the lower part (300–700 cm depth) is substantially higher than that in the upper part (100–300 cm depth). In desert environments, sedimentary hiatuses may occur within dune sequences due to strong wind erosion; thus, the lower sedimentation rate in the upper part of the profiles may be related to intensive and/or frequent aeolian erosion.

Table 2 Optically stimulated luminescence (OSL) dating results for the three sand dune profiles (GEB11, GEB12, and GEB15)

Sample No.	Depth (cm)	U-238 (Bg/kg)	Ra-226 (Bg/kg)	Th-232 (Bg/kg)	K-40 (Bg/kg)	Dose rate (Gy/ka)	De (Gy)	Age (a BP)
GEB11-1	100	19.5±6.1	13.3±0.5	15.9±0.5	391.5±13.8	1.9±0.1	0.6±0.04	300±100
GEB11-3	300	17.1±6.5	13.7±0.5	17.5±0.5	412.0±14.6	2.0±0.1	1.4±0.10	700±100
GEB11-5	500	21.1±6.0	13.4±0.5	16.1±0.5	405.4±0.5	1.9±0.1	1.4±0.10	800±100
GEB11-7	700	11.4±7.0	16.3±0.5	18.8±0.5	426.1±15.1	2.0±0.1	1.8±0.10	900±100
GEB12-2	100	21.8±6.7	16.0±0.5	20.2±0.5	415.7±14.7	2.1±0.1	0.8±0.09	400±100
GEB12-3	140	18.1±5.1	13.8±0.4	15.5±0.4	300.4±10.7	1.6±0.1	1.7±0.10	1000±100
GEB15-2	130	23.7±6.7	16.7±0.5	22.2±0.6	431.4±15.2	2.2±0.1	0.7±0.03	300±100
GEB15-3	160	42.0±7.6	21.9±0.6	31.4±0.7	282.6±10.9	2.6±0.1	2.9±0.10	1100±100

Note: Mean±SD. BP, Before Present.

3.2 Grain size results

The grain size composition of the sediments from profile GEB11 varies substantially, with the mean grain size ranging from 162.87 to 200.02 μm (Fig. 5a–e). The profile is dominated by fine

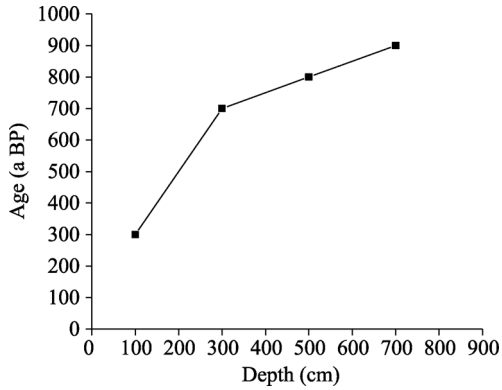

Fig. 4 Age-depth relationship for profile GEB11

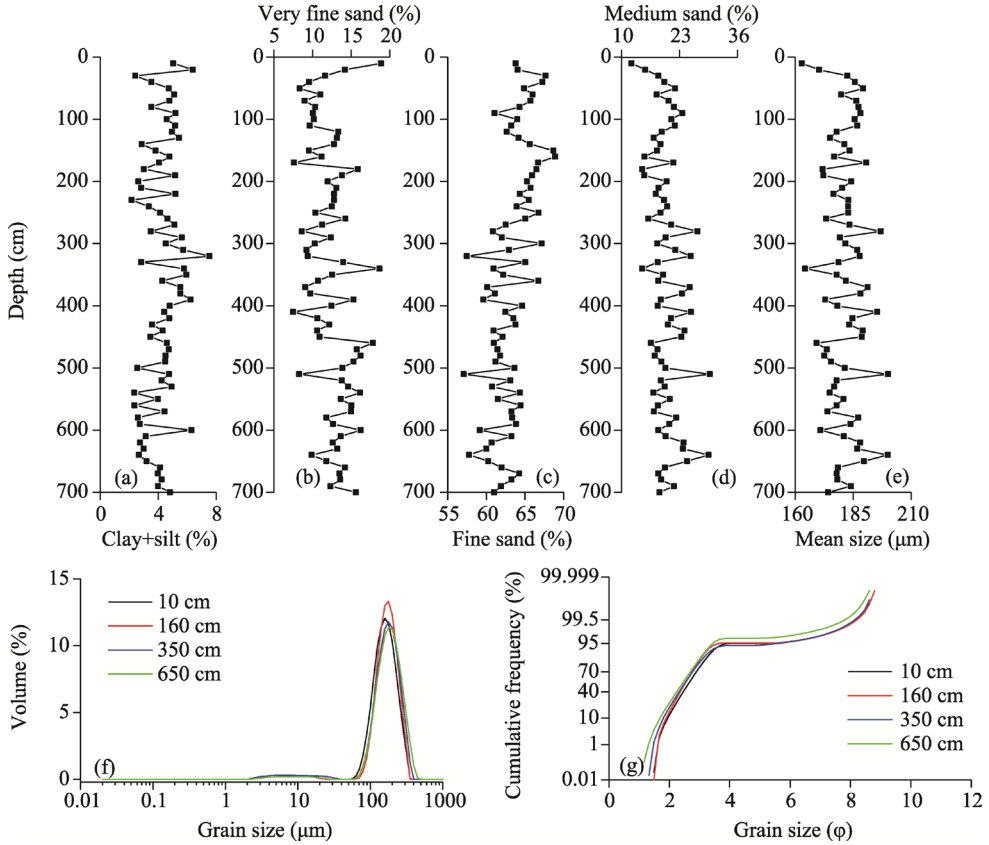

Fig. 5 Grain size results for profile GEB11. (a–d), depth profiles of clay+silt, very fine sand, fine sand, and medium sand fractions, respectively; (e), depth profile of the mean grain size; (f), grain size frequency distribution curves; (g), cumulative grain size frequency distribution curves.

sand, and the content ranges from 57.08% to 68.88% (average content of 63.62% (±2.56%)). In the lower part of the profile (400–700 cm depth), the proportion of fine sand is lower and relatively uniform. However, in the interval of 0–400 cm depth, the proportion of fine sand is higher and shows large fluctuations compared to the interval of 400–700 cm depth. The proportion of medium sand is the second highest within this profile, ranging from 12.26% to 28.87%. The proportion of very fine sand ranges from 7.50% to 18.89%, with the average of 12.43% (±2.60%). The fraction with gain size <63.00 μm (clay and silt) is a minor component in this profile (<7.54%).

Grain size frequency distribution curves of representative samples show a well-defined peak at approximately 150.00–180.00 μm and a minor peak at about 2.00–20.00 μm (Fig. 5f). Sediments deposited during a single sedimentation event or transported by a single transport process generally exhibit unimodal grain size frequency distribution curves. In contrast, multiple sedimentation events or transport processes may result in a polymodal distribution. The bimodal grain size frequency distributions of profile GEB11 suggest multiple transport processes or provenances. The cumulative probability curves indicate that the samples are dominated by the saltation dust components, together with minor suspension components (Fig. 5g), suggesting a relatively complex depositional process.

The results of the EM modeling analysis demonstrated that as the number of EMs increases, the goodness-of-fit statistics show an increasing quality of fit (higher R^2 and lower angular deviation). The three EMs provide a good fitting degree with a minimum number of EMs, with relatively high R^2 and low angular deviation values. Therefore, we chose a three-EM model to depict the particle sources and depositional processes of profile GEB11. The primary mode of end-member 1 (EM1) is about 126.00 μm. The abundance of this fraction ranges from 0.84% to 25.11% (Fig. 6a and b). End-member 2 (EM2) is the most abundant fraction throughout the profile, ranging from 63.12% to 91.54% with the primary mode at approximately 178.00 μm, representing fine sand. The abundance of EM2 is relatively stable within the interval of 400–700 cm depth, which is followed by an increasing trend from 400 cm depth to the top of the profile and culminates at the depth of about 150 cm. The interval of 0–150 cm depth has relatively high and fluctuating EM2 abundance, with two intervals having low values (100–150 and 0–30 cm depths) (Fig. 6a and c). The relative abundance of end-member 3 (EM3) varies between 0.00% and 29.20%, with the primary mode at approximately 283.00 μm, representing medium sand. EM3 shows a minor decreasing trend from the bottom to the top of the profile (Fig. 6a and d). It is noteworthy that the grain size frequency distribution curves show a peak at about 2.00–20.00 μm. However, the clay and silt EM cannot be observed in the results of the EM modeling analysis; this is because although these results express most of the grain size information (98.00% in this case), they do not provide all of this information. For profile GEB11, the proportion of the fraction with grain size <20.00 μm is minor (3.99%) and it was not extracted by the EM modeling analysis.

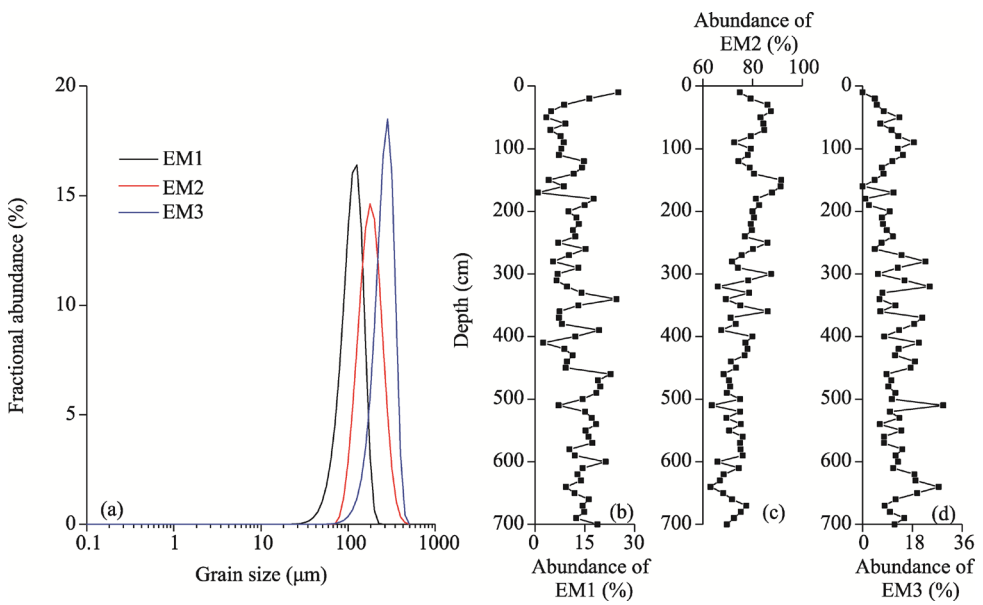

Fig. 6 Grain size frequency distribution curves of EM1–EM3 (a), and depth profiles of the abundance of EM1–EM3 (b–d). EM1, end-member 1; EM2, end-member 2; EM3, end-member 3.

4 Discussion

4.1 Significance of EMs as proxies of aeolian activity

The grain size range of EM1 varies from 11.20 to 283.00 μm, with the primary mode at approximately 126.00 μm and the mean size at 103.60 μm. EM1 is the only EM that contains the fine components. The fine components in aeolian deposits can be supplied to the site of deposition by three processes (Sun et al., 2004): (1) transported as discrete particles; (2) transported via attachment to larger grains or as aggregates (Pye, 1987; Tsoar and Pye, 1987); and (3) transported as a product of post-depositional pedogenesis (Bronger and Heinkele, 1990). In the study area, the influence of pedogenesis on sediments is negligible due to the hyper-arid climate (Chen et al., 2013). Therefore, the fine components are likely deposited via attachment to larger grains, or as aggregates, or carried by high-level circulation as discrete particles (Sun et al., 2004). On the Chinese Loess Plateau, the fine dust particles are deposited continuously; they represent the background dust aerosol on the Chinese Loess Plateau, and changes in these fine-grained components reflect variations in the westerly jet stream (Sun et al., 2004). The cumulative grain size probability curves indicate that the proportion of the suspension components in EM1 is about 11.00%, while EM2 and EM3 have almost no suspension components. This shows that EM1 is a mixture of suspension components and saltation dust, with a complex provenance (Fig. 7). The finest grain size of EM1 is 11.20 μm, which can be raised to the upper atmosphere under the action of strong winds and carried in suspension over thousands of kilometers in the air. Considering the wind regime and atmospheric circulation over the study area, we propose that the fine-grained components are transported in part by the Westerlies. Meanwhile, the saltation components of EM1 may be transported by strong winds, reflecting intense local aeolian activity (Qiang et al., 2007).

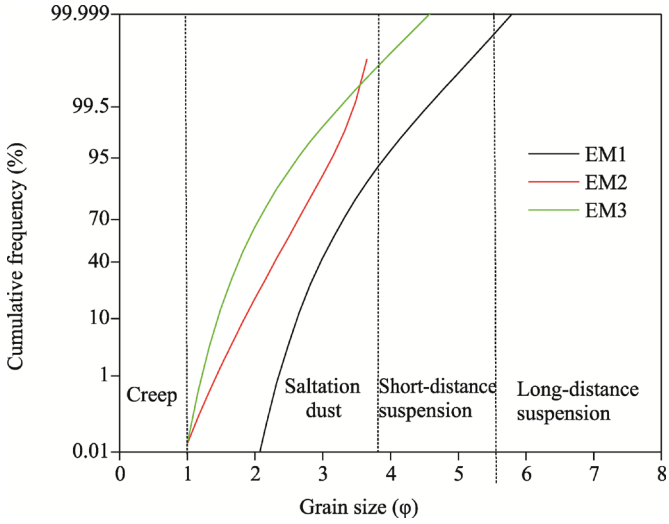

Fig. 7 Cumulative grain size probability curves of EM1, EM2, and EM3. As shown in this figure, EM1 represents a mixture of suspension and saltation dust, while EM2 and EM3 represent saltation dust.

EM2 and EM3 respectively represent fine sand and medium sand, with mean grain sizes of 167.98 and 241.52 μm, respectively; they are thus markedly coarser than EM1. Generally, compared to fine sediment, the transport distance of coarse sediment is shorter and requires a higher transport capacity (Qin et al., 2009). The cumulative grain size probability curves of EM2 and EM3 indicate that both fractions are mainly transported by saltation dust (Fig. 7). De Ploey (1977) and Lehmkuhl and Haselein (2000) argued that the transport capacity of most winds is sufficient to transport fine sand, and strong winds can transport medium sand by saltation. Previous studies have demonstrated that fine sand is the typical components of loess deposits that

have a local source (i.e., hundreds of meters to a few kilometers) (Pye, 1987; Sun et al., 2004; Vandenberghe, 2013). Examples include the loess deposits near river terraces along the Huangshui River (Vriend and Prins, 2005) and Yellow River (Prins et al., 2009) in China, and in the Mississippi Valley in the USA (Jacobs et al., 2011). Similarly, Li et al. (2018) suggested that the sand components (modal size of 180.00–560.00 μm) of loess on the eastern Tibetan Plateau is mainly transported by strong surface winds from the adjacent mountains and desertified areas. Vandenberghe (2013) illustrated the relationship between the grain size composition and transport distance of loess deposits at different sites worldwide, and the results confirmed that the loess deposits with the grain size >75.00 μm are mainly of local origin.

Li et al. (2002) and Wang et al. (2003) found that oasis soils are dominated by coarse silt and very fine sand, whereas desert sediments are dominated by fine sand. In the Taklimakan Desert of China, oasis sediments and desert sediments are dominated by EMs with the principal modal sizes of 5.00–30.00 and 200.00 μm, respectively (Liu et al., 2022). Additionally, grain size covaries with soil nutrients and geochemical ratios and it could be used to reflect desert expansion (i.e., intensive aeolian activity) (Liu et al., 2022). On the northern Qinghai-Tibet Plateau of China, Qiang et al. (2007) revealed that the changes in the sand fraction of the sediments in the Sugan Lake are controlled by the frequency of dust storms and strong winds. In addition, the fine sand components (modal size of 250.00 μm) of loess deposits from the Danube and Tisza rivers in Serbia (Bokhorst et al., 2011), the fine sand components (modal size of 158.90 μm) of loess deposits in the Mu Us Sandy Land of China (Liu et al., 2021), and the fine sand components (modal size of 174.62 μm) of the sediments in the Kumtagh Desert of China (Liang et al., 2020), can be regarded as the product of short-distance transport by strong near-surface winds. Thus, these components are a reliable proxy for detecting intensive aeolian activity, such as dust storm events.

As discussed above, in arid regions, the variation of coarse sediments (fine and medium sand) within stratigraphic profiles is mainly controlled by the intensity of aeolian activity or wind velocity. Thus, we propose that the coarse-grained components (EM2+EM3) of profile GEB11 was deposited in an arid environment with a strong wind regime, and it can be regarded as a proxy of aeolian activity in the southern Gurbantunggut Desert.

4.2 History of aeolian activity in the southern Gurbantunggut Desert and comparison with other areas

In this study, we used the changes in the coarse components, combined with the OSL chronology, to reconstruct the history of aeolian activity in the southern Gurbantunggut Desert during the past 900 a. As shown in Figure 8, the variations of the proxy of aeolian activity (i.e., EM2+EM3) for profile GEB11 showed three distinct stages during the last 900 a. The coarse-grained components (EM2+EM3) was more abundant during about 450–100 a BP (Before Present; corresponding to the LIA), indicating more frequent and intensive aeolian activity. By contrast, the coarse-grained components were less abundant during 900–450 a BP (corresponding to the MWP) and 100 a BP–present (corresponding to the Current Warm Period (CWP)), indicating weaker aeolian activity.

To provide a synthesis of the history of aeolian activity in Central Asia during the last 900 a, and to determine the mechanisms, we compared the results of profile GEB11 with multiple aeolian records of surrounding areas. In profiles GEB12 and GEB15, we observed that aeolian sand was deposited on the top of the fine silt and clay layers (Fig. 9). We conclude that this stratigraphic signature represents desert expansion events (i.e., more intensive aeolian activity). The OSL ages of the aeolian sand close to the fine silt and clay layers within profiles GEB12 and GEB15 are 400 (±100) and 300 (±100) a BP, respectively. Additionally, the OSL ages in the upper part of the clay layer are older than 1000 a BP (Fig. 9). This indicates that after the beginning of the LIA, the intensity or frequency of aeolian activity in the southern Gurbantunggut Desert was significantly enhanced. Based on four Holocene fluvial-lacustrine strata in the southern Gurbantunggut Desert, Ma (2005) demonstrated that the intensity or frequency of aeolian activity during the LIA was substantially higher than that during the MWP. This finding is consistent with our results of profile GEB11.

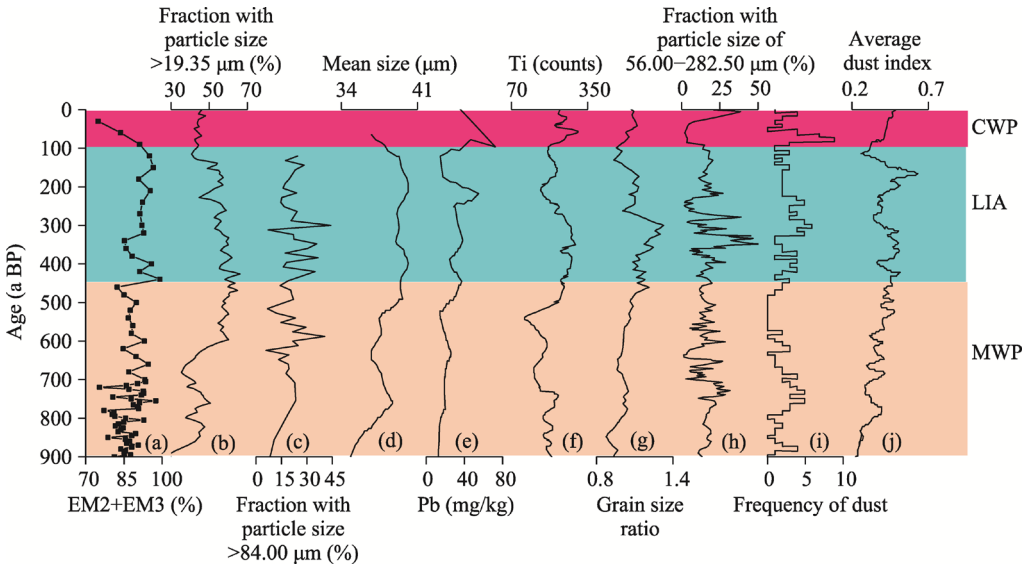

Fig. 8 Comparison of proxy age records of aeolian activity in Central Asia. (a), profile GEB11 in the southern Gurbantunggut Desert (this study); (b), fraction with grain size >19.35 μm in the sediments of the Bosten Lake, China (Zhou et al., 2019); (c), fraction with grain size >84.00 μm in the sediments of Yangchang loess profile from the southern margin of the Taklimakan Desert, China (Han et al., 2019); (d), mean grain size of the KMA loess profile on the northern slope of the Kunlun Mountains, China (Tang et al., 2009); (e), Pb concentration in the Halashazi peatland of the Altay Mountains, China (Xu, 2014); (f), Ti concentration in the sediments of the Aral Sea, Central Asia (Sorrel et al., 2007); (g), grain size ratio (ratio of grain sizes 6.00–32.00 μm to grain sizes 2.00–6.00 μm) in the Aral Sea, Central Asia (Huang et al., 2011); (h), fraction with grain size of 56.00–282.50 μm in the sediments of the Sugan Lake on the northern Qinghai-Tibet Plateau, China (Chen et al., 2013); (i), frequency of dust falls since 900 a BP (Before Present) (Zhang, 1984); (j), 50-a averaged synthesis dust storm record across the mid-latitude Asia (He et al., 2015). MWP, Medieval Warm Period; LIA, Little Ice Age; CWP, Current Warm Period.

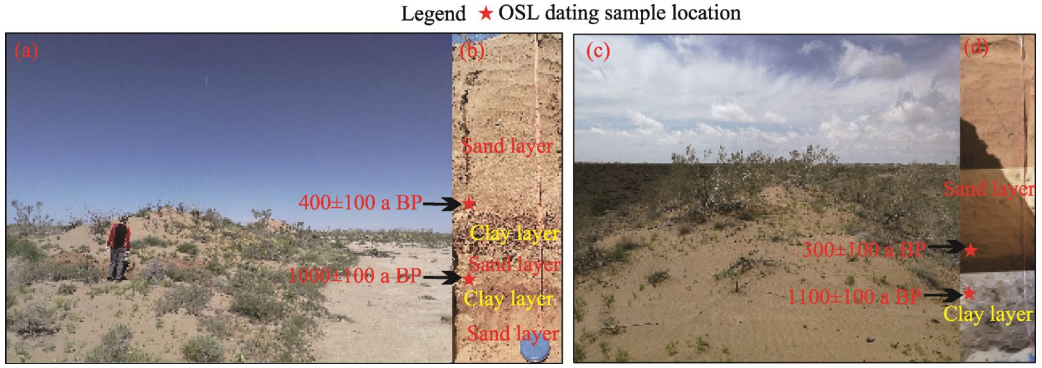

Fig. 9 Field photos showing the locations of optically stimulated luminescence (OSL) samples for sand dune profiles GEB12 (a–b) and GEB15 (c–d) in the southern Gurbantunggut Desert

Zhou et al. (2019) found that the fraction with grain size >19.35 μm in the sediments of the Boston Lake, China, can reflect the history of aeolian activity. The temporal variation of this fraction in the sediments of the Bosten Lake showed that during the past 2000 a, the most intensive aeolian activity was from 630 to 150 a BP, whereas the relatively weak aeolian activity occurred during 1540–630 a BP (Fig. 8b). Han et al. (2019) produced a continuous record of Holocene dust storm activity based on the sediments of Yangchang loess profile from the southern margin of the Taklimakan Desert. Changes in the coarse-grained components within this profile showed that, during the last 900 a, enhanced dust storm activity was synchronous with the LIA, while weaker dust storm activity occurred during the MWP (Fig. 8c). In the KMA loess profile on

the northern slope of the Kunlun Mountains in China, the loess deposits that accumulated during the LIA were coarser grained than those accumulated during the MWP, indicating more intense aeolian activity during the LIA (Tang et al., 2009; Fig. 8d).

More intense aeolian activity or dust storms resulted in an increased Pb concentration in peat deposits from the Altay Mountains, China (Xu, 2014). In the Halashazi peatland of Altay Mountains, markedly higher Pb concentrations occurred during 500–100 a BP, compared with those during 900–500 a BP, reflecting more intense aeolian activity during the LIA (Xu, 2014; Fig. 8e). In the Aral Sea, Ti concentration (Sorrel et al., 2007; Fig. 8f) and grain size ratio (ratio of grain sizes 6.00–32.00 μm to grain sizes 2.00–6.00 μm) (Huang et al., 2011; Fig. 8g) were used to traced airborne dust fluxes; both indicators showed that low aeolian deposition occurred during 1230–550 a BP (including the MWP), and exceptionally high aeolian deposition occurred from 550 a BP to the 1940s (including the LIA), with very low values after the 1940s.

In the Sugan Lake on the northern Qinghai-Tibet Plateau, the coarse-grained components (56.00–282.50 μm) was regarded as being wind-transported during dust storms (Chen et al., 2013). The abundance of the fraction with grain size of 56.00–282.50 μm in the sediments of the Sugan Lake indicated that, over the past 2000 a, intensive dust storms occurred during 450–250 a BP (Fig. 8h). Using Chinese historical records, Zhang (1984) reconstructed the decadal frequency of "dust-rain years" (i.e., dust fall events) since the AD 300 (AD, Anno Domini), and found that the atmospheric dust loading during the LIA was markedly higher than that during the MWP (Fig. 8i). He et al. (2015) produced a synthesis of dust storm records based on the average of standardized records from mid-latitude Asia, and showed that over the last 1000 a, more frequent dust storms occurred during cool periods, especially the LIA (Fig. 8j).

The consistency of the records of aeolian activity provided by profile GEB11 from the southern Gurbantunggut Desert with the records of aeolian activity from elsewhere in Central Asia confirms the existence of a coherent pattern of aeolian activity across the entire region of Central Asia during the last 900 a. Generally speaking, weaker aeolian activity occurred during the MWP, stronger aeolian activity during the LIA, and weaker aeolian activity again after approximately 100 a BP.

4.3 Possible forcing mechanisms of aeolian activity in Central Asia

Sand supply, vegetation cover (mainly related to soil moisture), and wind strength are the three principal factors controlling aeolian activity (Chen et al., 2013; Qiang et al., 2014, 2022; Han et al., 2019). We now assess the significance of each of these factors for the southern Gurbantunggut Desert. Ancient fluvio-lacustrine sediments are ubiquitous in the Junggar Basin, which are a major source of particles for dust emissions (Qian and Wu, 2010; Li et al., 2022). Therefore, sand supply should not be the dominant factor controlling the variations in aeolian activity.

Several researchers have proposed that climatic drying in arid and semi-arid regions may have driven the deterioration of the vegetation cover and the expansion of dust source areas (e.g., desert and Gobi), which increased the level of aeolian activity (Rea and Leinen, 1988; Guo et al., 2002). For instance, the coincidence of high dust accumulation in the Greenland ice cores (Zielinski and Mershon, 1997) and North Pacific sediments (Rea, 1994) with climatic drying in Asian dust source regions, supports this assumption, on glacial-interglacial timescale. The record of aeolian activity provided by profile GEB11 in this study (Fig. 10a) and comparable records from the surrounding areas confirm that the most intensive aeolian activity over the last 900 a occurred during the LIA, while aeolian activity was much weaker during the MWP and CWP. However, numerous studies have confirmed that in Central Asia, including the Junggar Basin, the humidity or precipitation was higher and the climate tended to become wetter during the LIA compared to the MWP (e.g., Chen et al., 2010; Fig. 10b). This suggests that the role of climatic drying in dust emissions may be overestimated. Additionally, Qiang et al. (2007) suggested that soil moisture and the vegetation cover have negligible impacts on dust emissions on the northeastern Qinghai-Tibet Plateau. The decreasing normalized difference vegetation index (NDVI) in Xinjiang implies that the increased precipitation during 1980–2020 did not cause an

increase in either soil humidity or the vegetation cover (Yao et al., 2021). This supports the conclusion that in the regions with low precipitation and high evaporation, a small amount of rainfall did not significantly increase the vegetation cover during the geological past.

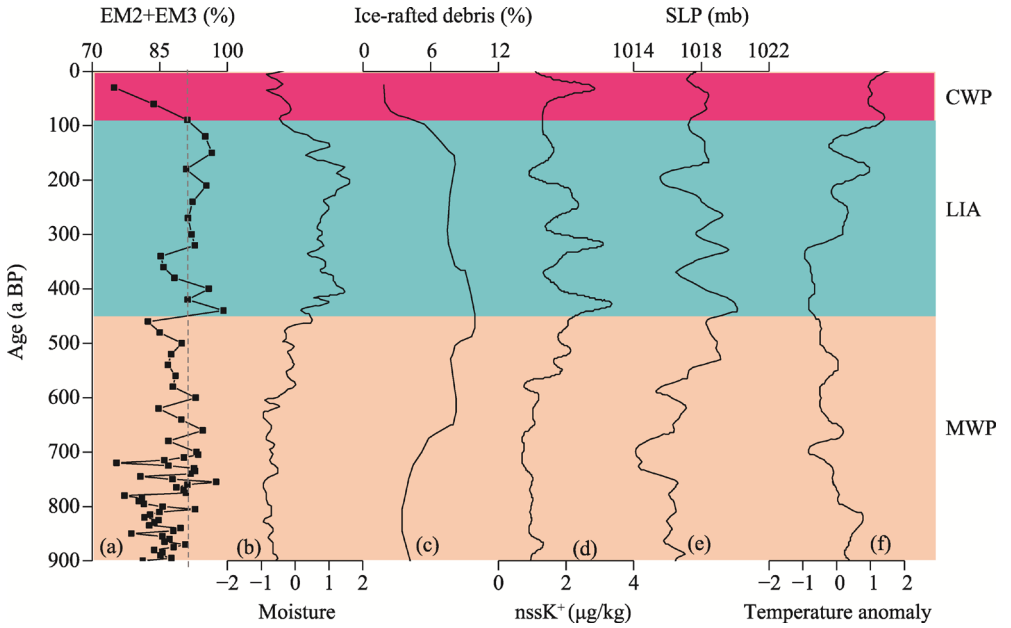

Fig. 10 Comparison of the records of aeolian activity in profile GEB11 in the southern Gurbantunggut Desert with possible driving mechanisms. (a), EM2+EM3 in profile GEB11 in the southern Gurbantunggut Desert; (b), synthesis of the records of effective moisture in Central Asia (Chen et al., 2010); (c), ice-rafted debris records from the North Atlantic (Bond et al., 1997); (d), non-sea salt ion (nssK$^+$) records from the GISP2 Greenland ice core (Mayewski and Maasch, 2006); (e), reconstruction of the strength of the Siberian High reflected by the sea-level pressure (SLP) over the North Atlantic and Asia (Meeker and Mayewski, 2002); (f), standardized temperature anomaly records for the western Central Asia (Esper et al., 2007).

Our record of aeolian activity is consistent with the ice-rafted debris events in the North Atlantic Ocean (Bond et al., 1997; Fig. 10c) and the record of the non-sea salt ions (nssK$^+$) in the GISP2 Greenland ice core (Mayewski and Maasch, 2006; Fig. 10d). This indicates that aeolian activity in Central Asia responded to abrupt climatic events at high northern latitudes and with global climate changes. This linkage on a large spatial scale reflects changes in atmospheric circulation, rather than local factors like the vegetation cover and precipitation. Kurosaki and Mikami (2003) and Liu et al. (2004) found a positive correlation between dust emission and surface wind velocity in northern China and argued that modern dust emissions are significantly controlled by surface wind velocity. A similar relationship between dust flux and wind surface velocity was observed in the northern Qaidam Basin on the Qinghai-Tibet Plateau (Qiang et al., 2007). Thus, we infer that in the geological past, the intensity and frequency of aeolian activity was driven by wind regimes, even during intervals with relatively wet climatic conditions, like the LIA. This conclusion is supported by modelling studies (e.g., Zhang et al., 2003), which indicate the dominant role of surface wind strength in desertification and dust emissions.

The study area is influenced by two atmospheric circulation systems: the Mongolian-Siberian High and the Westerlies. As shown in Figure 10e, during the last 900 a, aeolian activity in Central Asia was synchronous with changes in the Siberian High (Meeker and Mayewski, 2002). The Siberian High was relatively weak during the MWP, which is consistent with the low intensity of aeolian activity in Central Asia. By contrast, the Siberian High was greatly enhanced during the LIA, when intensive aeolian activity occurred. These observations suggest a causal linkage between the Siberian High and aeolian activity in Central Asia. Notably, the stages of the high intensity of aeolian activity coincided with the LIA, when the accumulation rate of the Guliya ice

core increased (Yao et al., 1996) and the $\delta^{18}O$ of Greenland ice cores decreased (Johnsen et al., 1992). These changes reflect the reduced global temperature during the LIA, including in Central Asia (Esper et al., 2007; Fig. 10f). By contrast, the reduced aeolian activity during the MWP and CWP coincided with relatively high temperatures, which indicates that temperature changes at high northern latitudes may have influenced aeolian activity in the study area. A teleconnection between aeolian activity in Central Asia and cold events at high northern latitudes has been proposed in previous studies (e.g., Sorrel et al., 2007; Huang et al., 2011; Han et al., 2019; Zhou et al., 2019). For instance, Qiang et al. (2014) found that aeolian activity in the Genggahai Lake on the northeastern Qinghai-Tibet Plateau coincided with the North Atlantic ice-rafting events during the Holocene, within the limits of the dating error. Cooling at high northern latitudes markedly enhances the intensity of the Siberian High, which is displaced southward as a result, causing the incursion of cold air masses from high northern latitudes, resulting in more robust wind regimes, and providing suitable conditions for dust emissions within the study area (An et al., 2011; Chen et al., 2013). Overall, we suggest that the enhanced Siberian High during cold periods, such as the LIA, has caused increases in aeolian activity and dust emissions in Central Asia, via the increased near-surface wind velocity.

As mentioned above, temperature has a significant influence on aeolian activity via its control of the intensity of the Siberian High and the wind regimes in Central Asia. Aeolian activity increased substantially during cold periods while decreased during warmer periods. Reference to Figure 9a shows a decrease in the coarse-grained components of profile GEB11 during the last 100 a, indicating a reduction in aeolian activity. During this interval, both instrumental and paleoenvironmental records show rising temperatures in the Northern Hemisphere (Moberg et al., 2005) and the long-term weakening of the Siberian High (Ding et al., 2014). In addition, dust storms in North Xinjiang have decreased during the last several decades (Fig. 2), consistent with the weakened Siberian High and increased temperatures in Central Asia. These observations support a coupled relationship between aeolian activity and temperature. Given the ongoing global warming trend, the relationship between aeolian activity and temperature is assumed to be maintained, and it is possible that the weakening of aeolian activity in Central Asia will continue (Kang et al., 2022). However, it is noteworthy that the factors driving aeolian activity are complex and changeable, and the impact of human activities especially must be considered, since it may exceed that of natural factors. For instance, Chen et al. (2013) found that dust storms recorded from the Sugan Lake were characterized by an abrupt increase in the mid-20th century, coincident with widespread petroleum exploitation from the 1950s onwards, which was regarded as the dominant driver of dust storms, as its disturbance of the ground surface leads to an increase in dust emissions.

It is important to acknowledge the limitations of profile GEB11 for constructing a high-resolution record of aeolian activity and climate change in the southern Gurbantunggut Desert. This is mainly due to the difficulty of accurate dating in the Gurbantunggut Desert given the lack of suitable organic materials (e.g., charcoal) for ^{14}C dating, and the relatively large error of OSL dating on the millennial-centennial timescale. However, our focus in this study is on two of the most significant climatic events (i.e., the LIA and MWP) during the last 900 a, and the determination of the response of aeolian activity to these events. The OSL chronology is sufficiently reliable to constrain these events within the profile, and the results of Ma (2005) support our conclusions. Nevertheless, more precise chronologies and studies of multiple locations and profiles are needed in the future to confirm our findings.

5 Conclusions

In this study, we produced a 900-a record of aeolian activity from a sedimentary sequence in the southern Gurbantunggut Desert in North Xinjiang, China. The coarse-grained components were used as an indicator of the intensity of aeolian activity. More intensive and frequent aeolian activity occurred during the LIA, while weakened aeolian activity occurred during the MWP and

CWP. The enhanced aeolian activity was associated with the strengthening of the Siberian High and cooling events at high northern latitudes in the Northern Hemisphere. Our results highlight the important role of the Siberian High in driving the intensity and frequency of aeolian activity in Central Asia, via temperature changes at high northern latitudes. Although weaker aeolian activity may occur in Central Asia in the future, under global warming scenarios, it is important to consider the direct impacts of human activities.

Acknowledgements

This study was supported by the National Natural Science Foundation of China (42167063), the Open Fund of Key Laboratory for Digital Land and Resources of Jiangxi Province (DLLJ202113), the State Scientific Survey Project of China (2017FY101001), the Natural Science Foundation of Jiangxi Province (20202BABL213028), and the Scientific Research Foundation of East China University of Technology (DHBK2019028). We thank the anonymous reviewers and editors for their valuable comments and Professor Jan BLOEMENDAL for language improvement.

References

An C B, Zhao J J, Tao S C, et al. 2011. Dust variation recorded by lacustrine sediments from arid Central Asia since ~15 cal ka BP and its implication for atmospheric circulation. Quaternary Research, 75(3): 566–573.

Bokhorst M, Vandenberghe J, Sümegi P, et al. 2011. Atmospheric circulation patterns in Central and Eastern Europe during the Weichselian Pleniglacial inferred from loess grainsize records. Quaternary International, 234(1–2): 62–74.

Bond G, Showers W, Cheseby M, et al. 1997. A pervasive millennial-scale cycle in North Atlantic Holocene and Glacial climates. Science, 278(5341): 1257–1266.

Booth B, Dunstone N J, Halloran P R, et al. 2012. Aerosols implicated as a prime driver of twentieth-century North Atlantic climate variability. Nature, 484(7393): 228–232.

Bronger A, Heinkele T. 1990. Mineralogical and clay mineralogical aspects of loess research. Quaternary International, 7–8: 37–51.

Chen F H, Chen J H, Holmes J, et al. 2010. Moisture changes over the last millennium in arid Central Asia: a review, synthesis and comparison with monsoon region. Quaternary Science Reviews, 29(7–8): 1055–1068.

Chen F H, Qiang M R, Zhou A F, et al. 2013. A 2000-year dust storm record from Lake Sugan in the dust source area of arid China. Journal of Geophysical Research: Atmospheres, 118(5): 2149–2160.

De Ploey J. 1977. Some experimental data on slopewash and wind action with reference to Quaternary morphogenesis in Belgium. Earth Surface Processes, 2(2–3): 101–115.

Ding Y H, Liu Y J, Liang S J, et al. 2014. Interdecadal variability of the East Asian winter monsoon and its possible links to global climate change. Journal of Meteorological Research, 28(5): 693–713.

Esper J, Frank D C, Wilson R J S, et al. 2007. Uniform growth trends among Central Asian low- and high-elevation juniper tree sites. Trees, 21(2): 141–150.

Fang X M, Li J J. 1999. Millennial-scale monsoonal climatic change from paleosol sequences on the Chinese western Loess Plateau and Tibetan Plateau: A brief summary and review. Chinese Science Bulletin, 44(S1): 38–52.

Ginoux P, Prospero J M, Torres O, et al. 2004. Long-term simulation of global dust distribution with the GOCART model: correlation with North Atlantic Oscillation. Environmental Modelling and Software, 19(2): 113–128.

Guo Z T, Ruddiman W F, Hao Q Z, et al. 2002. Onset of Asian desertification by 22 Myr ago inferred from loess deposits in China. Nature, 416(6877): 159–163.

Han W X, Lü S, Appel E, et al. 2019. Dust storm outbreak in Central Asia after ~3.5 kyr BP. Geophysical Research Letters, 46(1): 7624–7633.

He Y X, Zhao C, Song M, et al. 2015. Onset of frequent dust storms in northern China at ~AD 1100. Scientific Reports, 5(1): 17111, doi: 10.1038/srep17111.

Huang J P, Minnis P, Liu B, et al. 2006. Possible influences of Asian dust aerosols on cloud properties and radiative forcing observed from MODIS and CERES. Geophysical Research Letters, 33(6): L06824, doi: 10.1029/2005GL024724.

Huang X T, Oberhänsli H, Suchodoletz H, et al. 2011. Dust deposition in the Aral Sea: implications for changes in atmospheric

circulation in Central Asia during the past 2000 years. Quaternary Science Reviews, 30(25–26): 3661–3674.

Jacobs P M, Mason J A, Hanson P R. 2011. Mississippi Valley regional source of loess on the southern Green Bay Lobe land surface, Wisconsin. Quaternary Research, 75(3): 574–583.

Johnsen S J, Clausen H B, Dansgaard W, et al. 1992. Irregular glacial interstadials recorded in a new Greenland ice core. Nature, 359(6393): 311–313.

Kang S G, Wang X L, Wang N, et al. 2022. Siberian high modulated suborbital-scale dust accumulation changes over the past 30 ka in the Eastern Yili Basin, Central Asia. Paleoceanography and Paleoclimatology, 37(5): e2021PA004360, doi: 10.1029/2021PA004360.

Kurosaki Y, Mikami M. 2003. Recent frequent dust events and their relation to surface wind in East Asia. Geophysical Research Letters, 30(14): 1376, doi: 10.1029/2003GL017261.

Lehmkuhl F, Haselein F. 2000. Quaternary paleoenvironmental change on the Tibetan Plateau and adjacent areas (Western China and Western Mongolia). Quaternary International, 65(66): 121–145.

Li B S, Zhang D D, Zhou X J, et al. 2002. Study of sediments in the Yutian-Hotan Oasis, South Xinjiang, China. Acta Geological Sinica, 76(2): 221–228.

Li H J, Tang H. 2017. The circulation field characteristics of spring sandstorm in north Xinjiang in the extremely many years and few years. Desert and Oasis Meteorology, 11(1): 35–40. (in Chinese)

Li S, Yang S L, Liang M, et al. 2018. The end member model analysis on grain size of loess in the eastern Tibetan Plateau. Earth Environment, 46(4): 331–338. (in Chinese)

Li S H, Fan A C. 2011. OSL chronology of sand deposits and climate change of last 18 ka in Gurbantunggut Desert, northwest China. Journal of Quaternary Science, 26(8): 813–818.

Li Y, Song Y G, Kaskaoutis D G, et al. 2019. Atmospheric dust dynamics in southern Central Asia: Implications for buildup of Tajikistan loess sediments. Atmospheric Research, 229: 74–85.

Li Z Z, Jin J H, Liu Q, et al. 2022. Review and prospect of aeolian geomorphology research in Gurbantunggut Desert, China. Journal of Desert Research, 42(1): 41–47. (in Chinese)

Liang A M, Qu J J, Dong Z B, et al. 2020. The characteristic of grain size end members in Kumtagh Desert and its implication for sediment source. Journal of Desert Research, 40(2): 33–42. (in Chinese)

Liu B, Sun A J, Zhao H, et al. 2022. Physicochemical properties of surface sediments in the Taklimakan desert, northwestern China, and their relationship with oasis–desert evolution. CATENA, 208(4): 105751, doi: 10.1016/j.catena.2021.105751.

Liu R, Yue D P, Zhao J B, et al. 2021. Characteristics of grain size end members and its environmental significance of aeolian sand/loess sedimentary sequence since L2 in Hengshan, Shaanxi Province. Arid Land Geography, 44(5): 1328–1338. (in Chinese)

Liu X D, Yin Z, Zhang X Y, et al. 2004. Analyses of the spring dust storm frequency of northern China in relation to antecedent and concurrent wind, precipitation, vegetation, and soil moisture conditions. Journal of Geophysical Research: Atmospheres, 109: D16210, doi: 10.1029/2004JD004615.

Liu Z Y. 2020. The aeolian geomorphology and its development environment in Gurbantunggut Desert. MSc Thesis. Xi'an: Shannxi Normal University, 15–16. (in Chinese)

Lu H Y, Wang X H, Wang Y, et al. 2021. Chinese loess and the Asian monsoon: What we know and what remains unknown. Quaternary International, 620(4): 85–97.

Ma N N. 2005. Study of aeolian activity in the southern margin of Gurbantunggut Desert since Holocene. MSc Thesis. Beijing: University of Chinese Academy of Sciences, 55–57. (in Chinese)

Maher B A, Prospero J M, Mackie D, et al. 2010. Global connections between aeolian dust, climate and ocean biogeochemistry at the present day and at the last glacial maximum. Earth-Science Reviews, 99(1–2): 61–97.

Martin J H, Fitzwater S E. 1988. Iron deficiency limits phytoplankton growth in the north-east Pacific subarctic. Nature, 331(6154): 341–343.

Mayewski P A, Maasch K A. 2006. Recent warming inconsistent with natural association between temperature and atmospheric circulation over the last 2000 years. Climate of the Past Discussions, 2(3): 327–355.

McTainsh G, Strong C. 2007. The role of aeolian dust in ecosystems. Geomorphology, 89(1–2): 39–54.

Meeker L D, Mayewski P A. 2002. A 1400-year high-resolution record of atmospheric circulation over the North Atlantic and Asia. Holocene, 12(3): 257–266.

Middleton N J, Sternberg T. 2013. Climate hazards in drylands: A review. Earth-Science Reviews, 126: 48–57.

Moberg A, Sonechkin D M, Holmgren K, et al. 2005. Highly variable Northern Hemisphere temperatures reconstructed from low- and high-resolution proxy data. Nature, 433(7026): 613–617.

Paterson G A, Heslop D. 2015. New methods for unmixing sediment grain size data. Geochemistry, Geophysics, Geosystems, 16(12): 4494–4506.

Porter S C. 2001. Chinese loess record of monsoon climate during the last glacial-interglacial cycle. Earth-Science Reviews, 54(1–3): 115–128.

Prins M A, Zheng H B, Beets K, et al. 2009. Dust supply from river floodplains: the case of the lower Huang He (Yellow River) recorded in a loess–palaeosol sequence from the Mangshan Plateau. Journal of Quaternary Science, 24(1): 75–84.

Pye K. 1987. Dust and Dust Deposits. London: Academic Press, 1–78.

Qian Y B, Wu Z N. 2010. Environment of Gurbantunggut Desert. Beijing: Science Press, 1–128.

Qiang M R, Chen F H, Zhou A F, et al. 2007. Impacts of wind velocity on sand and dust deposition during dust storm as inferred from a series of observations in the northeastern Qinghai-Tibetan Plateau, China. Powder Technology, 175(2): 82–89.

Qiang M R, Liu Y Y, Jin Y X, et al. 2014. Holocene record of eolian activity from Genggahai Lake, northeastern Qinghai-Tibetan Plateau, China. Geophysical Research Letters, 41(2): 589–595.

Qiang M R, Lang W Z, He Z H, et al. 2022. A 1600-year record of eolian activity from Jili Lake in northern Xinjiang. Quaternary International, 631(C12): 93–104.

Qin X G, Cai B G, Mu Y, et al. 2009. A physical of loess dust transport process. Quaternary Science, 29(6): 1154–1161. (in Chinese)

Rea D K, Leinen M. 1988. Asian aridity and the zonal westerlies: Late Pleistocene and Holocene record of eolian deposition in the northwest Pacific Ocean. Palaeogeography, Palaeoclimatology, Palaeoecology, 66(1–2): 1–8.

Rea D K. 1994. The paleoclimatic record provided by eolian deposition in the deep sea: The geologic history of wind. Reviews of Geophysics, 32(2): 159–195.

Shin J Y, Hyeong K, Kim W. 2021. A sediment magnetic record in the North Pacific across the Mid-Pleistocene transition and its implication on Asian dust evolution. Frontiers in Earth Science, 9: 789584, doi: 10.3389/feart.2021.789584.

Sorrel P, Oberhänsli H, Boroffka N, et al. 2007. Control of wind strength and frequency in the Aral Sea basin during the late Holocene. Quaternary Research, 67(3): 371–382.

Su C J, Xu Z L, Zhang D L, et al. 2023. Aeolian and dust history since 14.4 cal. kyr BP indicated by grain size end members of Shayan loess in southern Kazakhstan. Quaternary Science, 43(1): 46–56. (in Chinese)

Sun D H, Bloemendal J, Rea D K, et al. 2004. Bimodal grain-size distribution of Chinese loess, and its palaeoclimatic implications. CATENA, 55(3): 325–340.

Tang Z H, Mu G J, Chen D M. 2009. Palaeoenvironment of mid-to late Holocene loess deposit of the southern margin of the Tarim Basin, NW China. Environmental Geology, 58(8): 1703–1711.

Tegen I, Lacis A A, Fung I. 1996. The influence on climate forcing of mineral aerosols from disturbed soils. Nature, 380(6753): 419–422.

Tsoar H, Pye K. 1987. Dust transport and the question of desert loess formation. Sedimentology, 34(1): 139–153.

Vandenberghe J. 2013. Grain size of fine-grained windblown sediment: A powerful proxy for process identification. Earth-Science Reviews, 121: 18–30.

Vriend M, Prins M A. 2005. Calibration of modelled mixing patterns in loess grain-size distributions: an example from the north-eastern margin of the Tibetan Plateau, China. Sedimentology, 52(6): 1361–1374.

Wang X M, Dong Z B, Zhang J W, et al. 2003. Grain size characteristics of dune sands in the central Taklimakan Sand Sea. Sedimentary Geology, 161(1–2): 1–14.

Wang X M, Dong Z B, Yan P, et al. 2005. Wind energy environments and dunefield activity in the Chinese deserts. Geomorphology, 65(1–2): 33–48.

Xu B, Wang L, Gu Z Y, et al. 2018. Decoupling of climatic drying and Asian dust export during the Holocene. Journal of Geophysical Research: Atmospheres, 123(2): 915–928.

Xu J Q. 2014. Holocene dust variability recorded by Alpine peat deposits in Altay Mountains, Northern Xinjiang. MSc Thesis. Lanzhou: Lanzhou University, 27–28. (in Chinese)

Yao J Q, Mao W Y, Chen J, et al. 2021. Signal and impact of wet-to-dry shift over Xinjiang, China. Acta Geographica Sinica,

76(1): 57–72. (in Chinese)

Yao T D, Thompson L G, Qin D H, et al. 1996. Variations in temperature and precipitation in the past 2000 a on the Xizang (Tibet) Plateau-Guliya ice core record. Science in China (Series D), 39(4): 425–433.

Yu P J, Xu H L, Zhang Q Q, et al. 2011. Change characteristics of sandstorm in the southern fringe of Gurbantunggut Desert since recent 49 years. Arid Land Geography, 34(6): 967–974. (in Chinese)

Zhang D E. 1984. Synoptic-climatic studies of dust fall in China since historic times. Scientia Sinica (Series B), 27(8): 825–836.

Zhang Q, Liu Q S, Li J H, et al. 2018. An integrated study of the eolian dust in pelagic sediments from the North Pacific Ocean based on environmental magnetism, transmission electron microscopy, and diffuse reflectance spectroscopy. Journal of Geophysical Research: Solid Earth, 123(5): 3358–3376.

Zhang X Y. 2001. Source distributions, emission, transport, deposition of Asian dust and loess accumulation. Quaternary Science, 21(1): 29–40. (in Chinese)

Zhang X Y, Gong S L, Zhao T L, et al. 2003. Sources of Asian dust and role of climate change versus desertification in Asian dust emission. Geophysical Research Letters, 30(24): 2272, doi: 10.1029/2003GL018206.

Zhou G P, Huang X Z, Wang Z L, et al. 2019. Eolian Activity history reconstructed by Bosten Lake grain size data over the past ~2 000 years. Journal of Desert Research, 39(2): 86–95. (in Chinese)

Zielinski G A, Mershon G R. 1997. Paleoenvironmental implications of the insoluble microparticle record in the GISP2 (Greenland) ice core during the rapidly changing climate of the Pleistocene-Holocene transition. Geological Society of America Bulletin, 109(5): 547–559.